SOCIETY OF PETROLEUM ENGINEERS OF AIME
6200 North Central Expressway
Dallas, Texas 75206

PAPER
NUMBER SPE 2037

Two-Phase Linear Fluid Flow Modeling for In Situ Combustion

By
D. H. Thurnau, Member AIME, Marathon Oil Co., Littleton, Colo.

This paper was prepared for the SPE Symposium on Numerical Simulation of Reservoir Performance to be held in Dallas, Tex., April 22-23, 1968. Permission to copy is restricted to an abstract of not more than 300 words. Illustrations may not be copied. The abstract should contain conspicuous acknowledgement of where and by whom the paper is presented. Publication elsewhere after publication in the JOURNAL OF PETROLEUM TECHNOLOGY or the SOCIETY OF PETROLEUM ENGINEERS JOURNAL is usually granted upon request to the Editor of the appropriate journal provided agreement to give proper credit is made.

Discussion of this paper is invited. Three copies of any discussion should be sent to the Society of Petroleum Engineers office. Such discussion may be presented at the above meeting and, with the paper, may be considered for publication in one of the two SPE magazines.

BACKGROUND

Considerable experimental and theoretical effort has been devoted to understanding the heat flow and stoichoimetric problems associated with the underground combustion process of oil recovery. Results of these efforts have been vital to success in the engineering of field applications of underground combustion.

Continued success in applying this process to diverse petroleum reservoirs would be aided by a quantitative understanding of the associated fluid flow phenomena. Semiquantitative notions (1, 2) about the oil displacement mechanisms and the nature of the "oil bank" are presently employed in the evaluation of underground combustion prospects. A quantitative delineation of the fluid flow aspects would facilitate better engineering predictions of:

1. Injectivity history (compressor requirements),
2. Sweep pattern,
3. Fuel content dependence on air flux.

A reasonably complete theoretical treatment of the in situ combustion process would require simultaneous solution of the heat flow, distillation, and three-phase fluid flow problems. Further, this should be done for a multidimensional medium which is not necessarily homogeneous or isotropic. While it is perfectly feasible to develop the necessary equations for such a model, their general solution was much too ambitious an undertaking for the computing capacity available when this work was begun.

We therefore confined this effort to exploring the numerical methods required and to becoming familiar with the displacement mechanisms that would be evidenced in the solution of a greatly simplified mathematical model. Specifically, the following restrictions were adopted:

1. Two-phase fluid flow (oil and air only).
2. No distillation effects.
3. Temperature profiles obtained from an independent study of the associated heat-flow problem.

To provide a basis for evaluating the results of the model study, a special laboratory tube run experiment was conducted. Here the sandpack was initially saturated with oil only, omitting the usual "connate" water. During burning, the only water present was the water of combustion. The experiments were conducted under psuedo-adiabatic conditions for which temperature distributions are known.

References, illustrations at end of paper.

Thus, the intent of the study was to compare experimental and theoretical results obtained with simultaneous air and oil flow in a linear homogeneous medium under conditions of superimposed temperature distributions associated with a moving heat source.

EVOLUTION OF MATHEMATICAL MODEL

A pictorial representation of the system to be studied is presented in Figure 1. The initial version of the fluid-flow model embodied the following features and limitations:

Oil and air flow only.

No immobile water present.

Air flux constant at input end.

Dead oil - incompressible.

No gravity drainage effects.

No capillary pressure effects.

Viscosities and air compressibility dependent on temperature.

Differential equations, which express conservation of the mass of oil and the mass of water, were developed around the above assumptions. These original equations, boundary conditions, and the methods used to solve them were not unlike those discussed in detail in Appendix A. Needless to say, the only hope for a solution lay in numerical methods, using a digital computer.

Physical properties for the finite difference model were chosen to correspond to a special 3-foot combustion tube experiment. The computer runs were made in two phases, corresponding to laboratory experimental practice. First, an extended air drive was done, starting with a high oil saturation in the sandpack. This was followed with the combustion phase of the run, which consisted of continuing the air drive at a lower flux and introducing temperature distributions corresponding to heat-up at the injection end and the advance of the flame front along the tube.

Three main effects were observed:

1. The air drive produced much lower oil saturations in the model than in the laboratory.

2. The "oil bank" that developed ahead of the flame front in the model had the characteristics of a shock front, i.e., a very sharp leading edge.

3. The "oil bank" in the model would grow in height, without a realistic lateral growth, until it was destroyed by instability.

These observations seemed to correlate with published results (3, 4, 5) on the effect of the capillary pressure term in the multiphase flow equations.

Addition of Gravity and Capillary Pressure Terms

These results necessitated a significant revision of the original model assumptions. Both capillary pressure and gravity terms were added to the flow equations. The effect of gravity was not expected to be important, even though the tube runs were done with vertically downward flow. This expectation was borne out.

Taking capillary pressure into account produced significantly different results in the combustion phase of the modeling. It eliminated the sharpness of the leading edge of the "oil bank", illustrated by the plots given in Figure 2. The problem with instability in the solution technique was considerably reduced. In fact, the instabilities could be eliminated by using the smallest grid increments that computer memory limitations would allow.

However, the problem of producing too much oil during the simulated air drive was still present. Unfortunately, this could readily be explained in terms of bypassing of air along the tube wall (in the actual experiment). The fraction of the air flux thus dissipated would undoubtedly change with temperature. This caused abandonment of any hope for quantitatively modeling the laboratory tube run.

Adoption of Dynamic, Nonuniform Grid Spacing

The saturation profiles that developed during modeling of the combustion phase were too steep to be properly represented on a practical-sized uniform grid. Various kinds of moving coordinate systems and/or coordinate transformations were considered. The difficulty was not resolvable by such techniques because there are multiple regions where fine grid is needed. Furthermore, the locations of these regions are not easily predicted. The problem was finally solved by the adoption of a dynamically adjusted nonuniform grid system. In this way, the grid was continually and automatically adapted to accurately represent the saturation function.

The details of the dynamics and use of nonuniform x-increments are spelled out in Appendix B. Besides dealing with high gradients of the dependent variables, such a grid system has one other important merit: it allows the total model length to be made quite large, without intolerable computer memory requirements.

Inclusion of Temperature-Dependent Capillary Pressure

A new problem appeared in the combustion phase results when capillary pressure was included in the model. The capillary pressure gradient at the leading edge of the "oil bank" contributed importantly to its development. However, at the trailing edge (not far from the flame front) the capillary pressure gradient was opposite in sign. This largely nullified the former effectiveness of the air pressure gradient in causing mobile oil to flow from the vicinity of the combustion front. The net effect was to leave an abnormally high quantity of oil behind.

The solution to the above problem lay in the temperature dependence of interfacial tension. Capillary pressure varies directly with interfacial tension and the latter decreases markedly with increasing temperature. Thus, it became necessary to regard capillary pressure as a function of both temperature and saturation. The actual functions used are described in Appendix C.

For a clearer understanding of the exact role and the importance of capillary pressure effects discussed above, we refer first to Figure 3. Here are plotted the three dependent functions of the model at a given point in time, against axial distance in the vicinity of the flame front. The point in time is such that the flame front has traveled 1.45 ft from the input face. This plot represents a portion of a successful solution using temperature-dependent capillary pressure. The leading edge of the "oil bank" is sharper than it is for the capillary pressure case in Figure 2. This is primarily because the flame front has advanced farther in Figure 3. It is also because less oil is being left behind, thus enlarging the "oil bank".

The oil pressure and capillary pressure curves are plotted in Figure 4 superimposed on the oil saturation curve from Figure 3. Shown there are both temperature-dependent and temperature-independent curves. Note that the gradient of the oil pressure without temperature dependence is reversed at a point high on the trailing edge of the "oil bank". This would cause counterflow of oil, thereby prohibiting a sharp trailing edge for the "oil bank" and resulting in the unrealistically high residual oil mentioned previously. It is evident that the "oil bank" seen in Figure 3 could never have formed without temperature-dependent capillary pressure.

Attempt to Simulate Tube Run

Figures 5, 6, and 7 present results that are typical of an attempt to simulate the tube run. An air flux of 100 standard cu ft/hr/sq ft was used.

Figure 5 presents results which are obtainable from the model only. It shows the manner in which the "oil bank" develops with time. In other runs, with greater "tube" lengths, it was found that the height of the "oil bank" and the shapes of the leading and trailing edges eventually stabilize. The height of the flat portion of the "oil bank" also stabilized, at a saturation level consistent with conventional multiphase flow concepts.

Figures 6 and 7 compare results that are common to the experimental and simulated runs. The lack of quantitative agreement is probably due to inadequacies of the model in not accounting for distillation effects, the presence of water of combustion, and likely air-bypassing.

CONCLUSIONS

Because of the simplifying assumptions of the mathematical model used in this study, we cannot reach any quantitative conclusions. However, there are several valid qualitative results:

1. Capillary forces play a significant role in "oil bank" development during in situ combustion.

2. The temperature dependence of capillary pressure is as important as its saturation dependence when high temperature gradients are present.

3. A dynamic nonuniform finite difference grid system has utility in the simulation (in one dimension) of displacement processes.

REFERENCES

1. Szasz, S. E. Evaluating the Heat Wave Process. World Oil, 89 (August 1, 1961).

2. Wilson, L. A., Wygal, R. J., Reed, D. W., Gergins, R. L., and Henderson, H. J. Fluid Dynamics During an Underground Combustion Process. Trans. AIME 216, 146 (1958).

3. Cardwell, W. T., Jr. The Meaning of the Triple Value in Noncapillary Buckley-Leverett Theory. Trans. AIME 216, 271 (1959).

4. Fayers, F. J. and Sheldon, J. W. The Effect of Capillary Pressure and Gravity on Two-Phase Fluid Flow in a Porous Medium. Trans. AIME 216, 147 (1959).

5. McEwen, C. R. A Numerical Solution of the Linear Displacement Equation with Capillary

Pressure. Trans. AIME 216, 412 (1959).

6. West, W. J., Garvin, W. W., and Sheldon, J. W. Solution of the Equations of Unsteady State Two-Phase Flow in Oil Reservoirs. Trans. AIME 201, 217 (1954).

7. Thurnau, D. H. Bandsolve - Algorithm Section. Communications of the Association for Computing Machinery 6, 441 (August, 1963).

8. Bailey, H. R. and Larkin, B. K. Convection-Conduction in Underground Combustion. Trans AIME 219, 320 (1960).

9. Corey, A. T. Interrelation Between Gas and Oil Relative Permeabilities. Producers Monthly 19, 38-41 (November, 1954).

10. Bikerman, J. J. Surface Chemistry; Theory and Applications. Academic Press (1958).

APPENDIX A

Equations for Oil-Gas Flow in a Linear Porous System

The development of the partial differential equations of fluid flow for a linear porous system containing only oil and gas begins with Darcy's law, written for any consistent system of units as follows:

$$\text{(Gas)} \quad V_g = - k_{rg} k \left(\frac{\partial}{\partial x} p_g + \rho_g g\right)/\mu_g \quad . \quad . \quad \text{(A-1)}$$

$$\text{(Oil)} \quad V_o = - k_{ro} k \left(\frac{\partial}{\partial x} p_o + \rho_o g\right)/\mu_o \quad . \quad . \quad \text{(A-2)}$$

where V = flux (volumetric flow rate per unit area normal to flow)

k_r = relative permeability
k = specific permeability
p = absolute pressure
ρ = density
g = gravity component in direction of flow
μ = viscosity of the flowing fluid.

Capillary forces relate the pressures p_g and p_o in the following manner:

$$p_g = p_o + P_c \quad , \qquad \text{(A-3)}$$

where P_c is the "capillary pressure". It was found necessary to regard P_c as a function of both temperature and saturation.

The relative permeabilities, k_{ro} and k_{rg}, are regarded as functions of oil saturation only.

Continuity equations may be written for each of the two flowing phases as

$$\frac{\partial}{\partial x} (V_g \rho_g) = - \phi \frac{\partial}{\partial t} (\rho_g S_g) \quad . \quad . \quad . \quad \text{(A-4)}$$

$$\frac{\partial}{\partial x} (V_o \rho_o) = - \phi \frac{\partial}{\partial t} (\rho_o S_o) \quad . \quad . \quad . \quad \text{(A-5)}$$

Terms arising from the solubility of gas in oil were not included in (A-4), above, where the gas of interest is air and the oil is assumed to be "dead". Further, the oil phase was treated, as an incompressible fluid, making ρ_o constant. The gas density, ρ_g, was assumed to vary according to the ideal gas law. Thus,

$$\rho_g = \rho_i \frac{p_g}{p_i} \frac{T_i}{T} \quad , \qquad \text{(A-6)}$$

where the subscript i denotes initial conditions.

Because oil and gas are considered to be the only fluids present in the porous medium, it follows that

$$S_g + S_o = 1. \qquad \text{(A-7)}$$

Taking these conditions and definitions into account in equations (A-4) and (A-5), combined with (A-2) and (A-3), leads to the final form of the linear multiphase flow equations:

$$\frac{\partial}{\partial x} \left(\frac{k_{rg} kp}{\mu_g T} \left(\frac{\partial p}{\partial x} + \frac{p}{T} \rho_g g \right) \right) = \phi \frac{\partial}{\partial t} \frac{p(1-S)}{T} \qquad \text{(A-8)}$$

$$\frac{\partial}{\partial x} \left(\frac{k_{ro} k}{\mu_o} \left(\frac{\partial p}{\partial x} - \frac{\partial P_c}{\partial x} \rho_i g \frac{T_i}{p_i} \right) \right) = \phi \frac{\partial S}{\partial t} \qquad \text{(A-9)}$$

where "o" and "g" subscripts have now been dropped, so that p represents gas pressure and S represents oil saturation.

Using the relationship

$$\frac{\partial P_c}{\partial x} = \frac{\partial P_c}{\partial S} \frac{\partial S}{\partial x} + \frac{\partial P_c}{\partial T} \frac{\partial T}{\partial x} \qquad \text{(A-10)}$$

Equation (A-9) may be more meaningfully written as

$$\frac{\partial}{\partial x} \left(\frac{k_{ro} k}{\mu_o} \left(\frac{\partial p}{\partial x} - \frac{\partial P_c}{\partial S} \frac{\partial S}{\partial x} - \frac{\partial P_c}{\partial T} \frac{\partial T}{\partial x} + \rho_i g \frac{T_i}{p_i} \right) \right)$$

$$= \phi \frac{\partial S}{\partial t} \, . \qquad \text{(A-11)}$$

For numerical solution, it is necessary to have finite difference analogs for the above partial differential equations. The space grid is

assumed to be nonuniform as described in Appendix B. The space increments actually to be associated with each grid point in the difference equations can be computed from a general equation, corresponding to Equations (B-2),

$$\Delta x_m = (Dx_{m-1} + 2 \cdot Dx_m + Dx_{m+1})/4. \quad \text{(A-12)}$$

With the diagrams of the difference grid, given in Appendix B, in mind, Equations (A-8) and (A-11) can be written as a pair of difference equations for each grid increment. For the finite increment m, this pair of equations for the time interval t to t + Δt would be as follows:

$$\frac{1}{\Delta x_m}\left(\left(\frac{k_{rg}k_p}{\mu_g T}\left(\frac{\partial p}{\partial x} + \frac{p\rho_g g}{T}\right)\right)_{\substack{x=x_m^+ \\ t=t+\Delta t}} - \left(\frac{k_{rg}k_p}{\mu_g T}\left(\frac{\partial p}{\partial x} + \frac{p\rho_g g}{T}\right)\right)_{\substack{x=x_m^- \\ t=t+\Delta t}}\right)$$

$$= \frac{\phi}{\Delta t}\left((p(1-S)_{\substack{x=x_m \\ t=t+\Delta t}} - (p(1-S))_{\substack{x=x_m \\ t=t}}\right) \quad \text{(A-13)}$$

$$\frac{1}{\Delta x_m}\left(\left(\frac{k_{ro}k}{\mu_o}\left(\frac{\partial p}{\partial x} - \frac{\partial P_c}{\partial S}\frac{\partial S}{\partial x} - \frac{\partial P_c}{\partial T}\frac{\partial T}{\partial x} + \rho_i g \frac{T_i}{p_i}\right)\right)_{\substack{x=x_m^+ \\ t=t+\Delta t}} - \left(\frac{k_{ro}k}{\mu_o}\left(\frac{\partial p}{\partial x} - \frac{\partial P_c}{\partial S}\frac{\partial S}{\partial x} - \frac{\partial P_c}{\partial T}\frac{\partial T}{\partial x} + \rho_i g \frac{T_i}{p_i}\right)\right)_{\substack{x=x_m^- \\ t-t+\Delta t}}\right)$$

$$= \frac{\phi}{\Delta t}\left(S_{\substack{x=x_m \\ t=t+\Delta t}} - S_{\substack{x=x_m \\ t=t}}\right) \quad \text{(A-14)}$$

x_m^+ refers to the midpoint between points m+1 and m. Similarly, x_m^- is midway between points m and m-1.

The increment boundaries are always midway between adjacent grid points, which are at the midpoints of their corresponding Dx's. This allows the difference approximation for a derivative taken at an increment boundary to be derived in the usual way. Thus, we have

$$\left(\frac{\partial p}{\partial x}\right)_{x=x^+} = 2 \cdot (p_{m+1} - p_m)/(Dx_m + Dx_{m+1}). \quad \text{(A-15)}$$

$$\left(\frac{\partial p}{\partial x}\right)_{x=x^-} = 2 \cdot (p_m - p_{m-1})/(Dx_{m-1} + Dx_m) \quad \text{(A-16)}$$

$$\left(\frac{\partial S}{\partial x}\right)_{x=x^+} = 2 \cdot (S_{m+1} - S_m)/(Dx_m + Dx_{m+1}) \quad \text{(A-17)}$$

$$\left(\frac{\partial S}{\partial x}\right)_{x=x^-} = 2 \cdot (S_m - S_{m-1})/(Dx_{m-1} + Dx_m) \quad \text{(A-18)}$$

Equations (A-15) through (A-18) are combined with Equations (A-13) and (A-14) to obtain the final finite difference equations for numerical solution.

In this work, analytical expressions were used to approximate the empirical functions k_{ro}, k_{rg}, μ_o, μ_g, and P_c. The temperature profile was also described analytically. All of these are discussed further in Appendix C.

Solution of the set of finite difference equations, with appropriate boundary conditions, was done with Newton iteration within each time step. (All coefficients and finite differences were evaluated at the midpoint of the time step.) Saturations and pressures for the new time level were obtained by solution of simultaneous equations set up to form a band matrix in the manner of West, Garvin and Sheldon (6). The resulting band matrix was solved by Gaussian elimination, using an algorithm published by the author (7).

APPENDIX B

Dynamic Nonuniform Space Grid

The numerical solution of partial differential equations may be accomplished by computing values for the dependent variable(s) by finite difference schemes. The success of this scheme depends on using sufficiently small increments of time, Δt, and distance, Δx, between points in the space grid. However, the demands on computer time and storage are rapidly increased as these increments are made smaller.

In many problems it is necessary to let Δt be automatically adjusted according to the current values of time derivatives of the dependent variables at certain points in space. There are other problems in which a nonuniform space grid is essential. This is usually accomplished by means of a transformation of the space coordinates. Further, the space region of interest may change with time, often leading to the adoption of a moving coordinate system (which implies that suitable moving boundary conditions can be defined).

All of these complications are present in the solution of in situ combustion fluid flow

equations. A space grid that could move with the flame front would seem desirable. This moving grid should also be nonuniform in order to allow an accurate representation of the dependent variables in regions where their space derivatives are high. The location of these regions is not easily predicted, however.

An unconventional solution to the problem of providing a suitable space grid was used here. This consisted of a dynamic, nonuniform space grid wherein, at every point in time, the grid density is locally adjusted. The basic scheme is (1) to subdivide the x increment at any point where the product $Dx \frac{\partial S_o}{\partial x}$ becomes greater than a specified maximum and (2) to recombine x increments at places where $Dx \frac{\partial S_o}{\partial x}$ falls below a specified minimum. The dependent variable S_o is monitored because high values of its space derivative are associated with transients in the fluid distribution ahead of the flame front.

The derivation of the difference equations has to take into account nonuniform space grid. This requires keeping a record of all current Dx values, corresponding to current values of the dependent variables, p_g and S_o. Thus, any adjustment of the space grid has to be accompanied by appropriate corresponding adjustments of the p_g and S_o records.

A decision to split a given Dx in two, based on the saturation gradient criterion alone, led to situations where adjacent Dx's were more than a factor of two different in magnitude. This causes doubt about the validity of the finite difference analog in the region of these points. A third criterion governing the decision to subdivide a given Dx was found adequate, namely, that it would not occur if either Dx adjacent to the increment in question were larger.

In recombining x increments in regions where the saturation gradient is sufficiently low, two simple additional criteria are needed: (1) that the two increments in question are equal in size and (2) that adjacent to one of them must be an increment of larger size. Special conditions are needed at the boundaries. One of these is that no recombination occurs if the increments are already up to the original, maximum, size. This insures that proper pairs will always be recombined to reinstate the grid to uniform, maximum-sized, increments when the saturation gradient approaches zero.

In deriving formulas for computing new saturation values at newly adjusted points in the grid, two physical requirements are imposed. One is essentially conservation of mass, i.e. the integral of the saturation function over the region affected must be invariant. The other is to preserve the gradient of both pressure and saturation in the region affected.

However, these requirements are not sufficient until recognition is made of the physical significance of the nonuniform finite difference grid. The use of valid finite difference methods to solve partial differential equations is indistinguishable from the solution of a set of difference equations derived from the physical concepts behind the partial differential equations. Thus we are led to the association of a unit cell with each point in space for which values of the dependent variables are to be computed.

In terms of the present linear model, the following diagram is relevant.

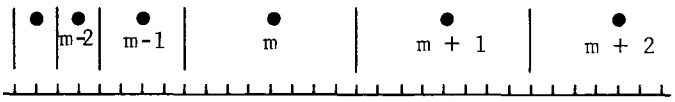

The grid points m, m+1 and m+2 are the midpoints of the three space increments Dx_m, Dx_{m+1}, and Dx_{m-2}, where $Dx_{m-1} = Dx_m/2$ and $Dx_{m-2} = Dx_{m-1}/2$, since these increments are a result of repeated binary splittings of the original increment to the left of increment m.

The question must be raised as to whether it is appropriate physically to locate the grid points m-2, m-1 and m at the midpoints of their space increments, since it is at these points (in space) that values of the dependent variables P and S are to be computed. Eventually, we must compute derivatives of the dependent variables at the increment boundaries. Would it be better to locate the grid point m-1 somewhere other than at the midpoint of the interval? Or would it be better to move the boundaries of the increment slightly? Such questions normally do not arise in working with a uniform space grid.

Difference analogs for space derivatives that are second-order accurate are readily derived for a uniform grid. Second order accuracy can be similarly maintained in this nonuniform grid by leaving the grid points at the center of their natural increments but shifting the boundary between actual increments such that it is midway between adjacent grid points. These boundaries are shown in the following diagram, where the solid lines show the actual boundaries between increments, and the dotted lines show the unshifted boundaries obtained from binary splittings of the original grid increments.

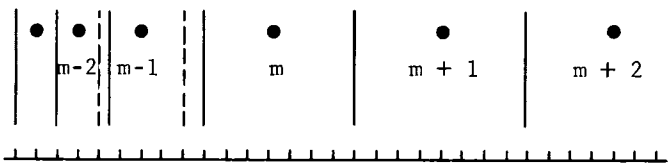

Thus, the width of the actual increment m-2 is

$$Dx_{m-2}/2 + (Dx_{m-1} + Dx_{m-2})/4,$$

and the width of the actual increment m-1 is

$$(Dx_{m-1} + Dx_{m-2})/4 + (Dx_m + Dx_{m-1})/4.$$

Having the grid points off-center in their actual space increments might appear strange. This situation arises in making the transition between regions of different-sized uniform increments. Such transitions are associated with nonzero second derivatives of the saturation function. In such regions, the off-center grid points offer at least as much accuracy as centered points in representing the average saturation of their respective increments. This is seen qualitatively in the following diagrams, where the area under the horizontal line should ideally equal the area under the curve.

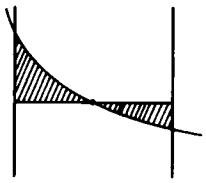
NATURAL GRID INCREMENT

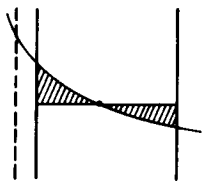
SAME INCREMENT WITH SHIFTED BOUNDARY

Only four cases arise in deriving formulas for computing new saturation values when a given space increment is split. One of these cases is presented by the diagram

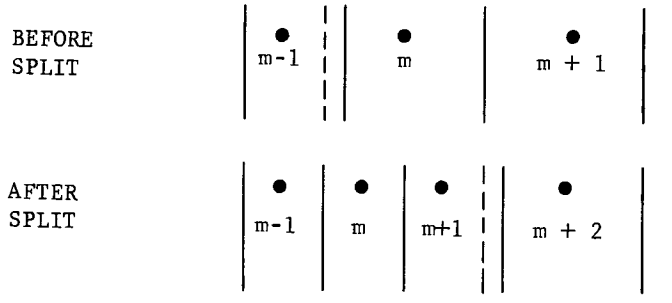

Using primes to denote the situation after splitting, we can relate the natural increment sizes as follows:

$$Dx_{m-1} = Dx_m/2 = Dx_{m+1}/2 = Dx'_{m+2}/2 = Dx'_{m+1} = Dx'_m = Dx'_{m-1} \quad \ldots\ldots\ldots \text{(B-1)}$$

By inspection, the actual increment sizes can be written as follows:

$$\begin{aligned}
\Delta x_{m-1} &= Dx_{m-1}/2 + (Dx_m + Dx_{m-1})/4 \\
\Delta x_m &= Dx_m/2 + (Dx_m + Dx_{m-1})/4 \\
\Delta x_{m+1} &= Dx_{m+1} \\
\Delta x'_{m-1} &= Dx'_{m-1} \\
\Delta x'_m &= Dx'_m \\
\Delta x'_{m+1} &= Dx'_{m+1}/2 + (Dx'_{m+1} + Dx'_{m+2})/4 \\
\Delta x'_{m+2} &= Dx'_{m+2}/2 + (Dx'_{m+1} + Dx'_{m+2})/4
\end{aligned} \quad \ldots \text{(B-2)}$$

Since the former increment m is the one being split, the saturation values S_{m-1} and S_{m+1} are to be retained without change. However, the former m+1 increment gets renumbered m+2. Thus,

$$S_{m-1} = S'_{m-1} \text{ and } S_{m+1} = S'_{m+2}. \quad \ldots \text{(B-3)}$$

The derivation of formulas for S'_m and S'_{m+1} is accomplished by writing the following two equations, expressing conservation of mass separately on each side of the former point m:

$$\begin{aligned}
S_{m-1} \cdot Dx_m/8 + S_m \cdot 3 \cdot Dx_m/8 &= S'_m \cdot Dx'_m \\
S_m \cdot Dx_m/2 + S_{m+1} \cdot Dx_{m+1}/8 &= S'_{m+1} \cdot Dx'_{m+1}/2 \\
&\quad + S'_{m+1} \cdot 3 \cdot Dx'_{m+1}/4.
\end{aligned} \quad \ldots \text{(B-4)}$$

After substitution to eliminate all Dx''s plus suitable algebra, these can be resolved to the two formulas:

$$\begin{aligned}
S'_m &= (S_{m-1} + 3 \cdot S_m)/4 \\
S'_{m+1} &= (S_{m+1} + 4 \cdot S_m)/5. \quad \ldots \text{(B-5)}
\end{aligned}$$

Now, we define two quantities T_1 and T_2 as:

$$\begin{aligned}
T_1 &= 2 \cdot (1 + Dx_{m-1}/Dx_m) \\
T_2 &= 2 \cdot (1 + Dx_{m+1}/Dx_m). \quad \text{(B-6)}
\end{aligned}$$

This allows writing equations (B-5) as

$$\begin{aligned}
S'_m &= (T_1 \cdot S_m + S_{m-1})/(T_1 + 1) \\
S'_{m+1} &= (T_2 \cdot S_m + S_{m+1})/(T_2 + 1) \quad \text{(B-7)}
\end{aligned}$$

The advantage is that these formulas cover the other three cases:

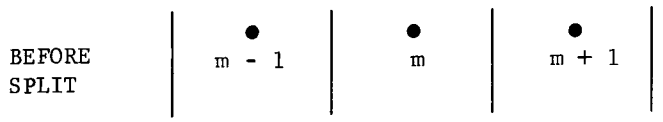

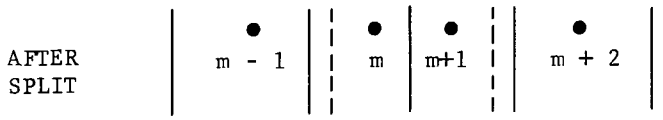

$$Dx_m = Dx_{m+1} = Dx_{m-1} = Dx'_{m-1} = 2 \cdot Dx'_m = 2 \cdot Dx'_{m+1} = Dx'_{m+2}.$$

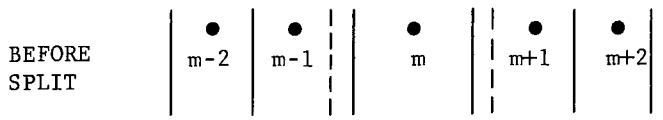

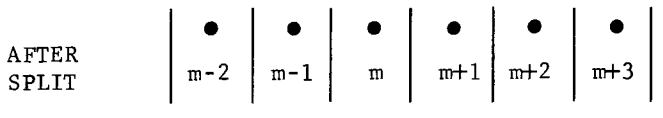

$$Dx_m/2 = Dx_{m+1} = Dx_{m-1} = Dx'_{m-1} = Dx'_m = Dx'_{m+1} = Dx'_{m+2}.$$

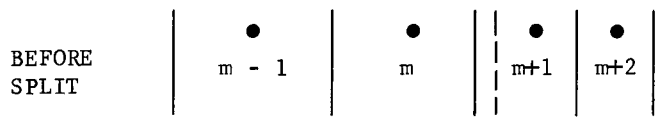

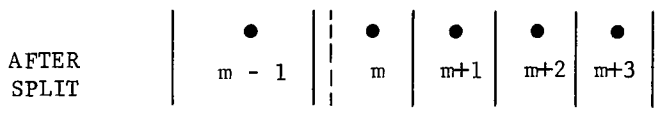

$$Dx_m = Dx_{m-1} = 2 \cdot Dx_{m+1} = Dx'_{m-1} = 2 \cdot Dx'_m = 2 \cdot Dx'_{m+1} = 2 \cdot Dx'_{m+2}.$$

When two grid elements are to be rejoined, a similar formula, derived in a manner analogous to that above is needed. Assuming the affected grid elements (before rejoining) are Dx_{m-1} and Dx_m, the formula for the "new" saturation is

$$S'_{m-1} = \frac{T_3 \cdot S_{m-1} + T_4 \cdot S_m - S_{m-2} - S_{m+1}}{T_3 + T_4 - 2} \quad \text{(B-8)}$$

where

$$T_3 = 3 + Dx_{m-2}/Dx_{m-1}$$

$$T_4 = 3 + Dx_{m+1}/Dx_m \quad \text{. . . .} \quad \text{(B-9)}$$

Recall the requirements that $Dx_{m-1} = Dx_m$ and that either $Dx_{m-1} = Dx_{m-2}/2$ and/or $Dx_m = Dx_{m+1}/2$. The three possible cases covered by the above formula may be diagrammed as follows:

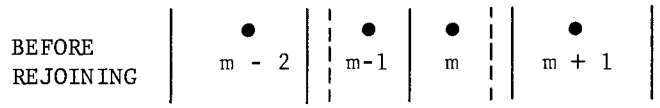

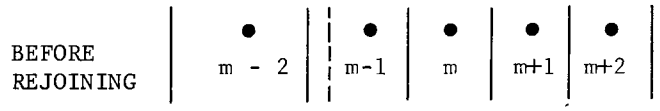

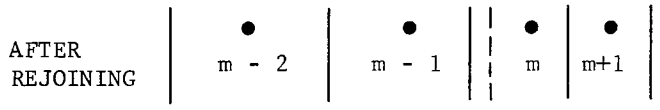

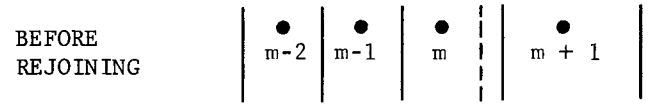

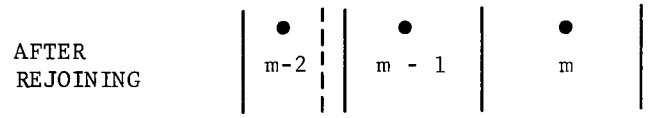

Completely analogous formulas are used for computing new pressure values when the grid is split or rejoined.

The adjustment criteria and formulas presented above are incorporated into an algorithm for maintaining a suitable nonuniform linear grid. This algorithm is applied to the current tabulations of the pressure and saturation functions at the end of each time step. More than one pass is often needed to obtain the correct adjustments. It is considered mandatory to split the grid whenever two adjacent saturation values are different by more than a set amount, ΔS_{max}. Rejoining is allowed whenever adjacent saturation differences are less than ΔS_{min}. Usually, it is best to have ΔS_{min} no larger than $\Delta S_{max}/4$. Typical values might be $\Delta S_{min} = .02$ and $\Delta S_{max} = .005$.

A higher level of control over the grid adjustment algorithm can be attained by programmatic modification of ΔS_{max} and ΔS_{min}. This is sometimes desirable in special circumstances such as a need to reduce redundant computing over stable regions such as that behind the combustion front.

APPENDIX C

Assumed Functions

In Appendix A there occur several parameters which are taken to be known functions. These describe physical characteristics of both the porous medium and the fluids. The purpose of this appendix is to show the actual empirical relationships that were used in this study. Since the heat flow problem was not solved as a part of this study, the means of obtaining temperature profiles will also be presented.

Temperature Profile

Bailey and Larkin (8) presented a solution to the case of heat flow with a moving heat source in an adiabatic, linear flow system. These are the conditions approximated in a laboratory tube run. The temperature distribution ahead of the flame front is given by an equation which is a simple approximation of Bailey and Larkin's results:

$$T = (T_f - T_a) \exp(-KVx) + T_a, \qquad (C\text{-}1)$$

where T_f = front temperature,

T_a = ambient temperature,

K = velocity constant,

V = air flux (std cu ft /hr /sq ft),

x = distance from the front (ft)

A value of 0.0437 was used for K, corresponding to a fuel content of roughly 2 pounds per cubic foot.

In this work, the temperature behind the front was held constant at the front temperature. The front temperature, after ignition, was held at 807 degrees F. During heat-up, the "front temperature" was increased linearly with time at a rate of 275 degrees per hour.

A typical temperature profile is shown in Figure C-1, along with oil viscosity data.

Fluid Viscosity

Air viscosity, as a function of temperature, was approximated by

$$\mu_g = 0.006876 + 0.0000204\ T. \quad . \quad . \quad (C\text{-}2)$$

where T is in degrees Rankin. Although more accurate formulas are available, the additional computing that they entail did not seem to be justified.

Oil viscosity, which varies markedly with temperature, was computed according to the standard A.S.T.M. correlation:

$$\log \log (\upsilon + 0.6) = A \log T + B \qquad (C\text{-}3)$$

The coefficients, A and B, were computed from experimental measurements of υ (kinematic viscosity) versus T (absolute temperature).

Figure C-1 shows a typical variation of oil viscosity in the region ahead of the flame front. The temperature profile corresponds to a front velocity of 0.25 feet per hour.

Relative Permeabilities

Relative permeabilities were computed from empirical formulas of the type developed by Corey (9):

$$k_{ro} = S_{oe}^4 \quad . \quad . \quad . \quad . \quad . \quad . \quad . \quad . \quad . \quad . \quad . \quad . \quad . \quad (C\text{-}4)$$

$$k_{rg} = (1 - S_{oe}^2)(1 - S_{oe})^2 \quad . \quad . \quad . \quad . \quad (C\text{-}5)$$

where

$$S_{oe} = \frac{\text{oil saturation - residual oil saturation}}{(1 - \text{residual oil saturation})} \qquad . \quad . \quad . \quad (C\text{-}6)$$

These approximate the characteristics of sand packs reasonably well if very low (0.1 or less) values for residual oil saturation are used.

Capillary Pressures

$$\text{Capillary Pressure} = \frac{1}{(1\text{-residual oil saturation})^2} \qquad . \quad . \quad . \quad (C\text{-}7)$$

in units of psi.

The above formula has validity only at room temperatures. To take into account the dependence of interfacial tension on temperature, the multiplicative factor

$$\frac{978\text{-}T}{448},$$

where T is in degrees Rankin was used. This factor is based on data and formulas given by Bikerman (10). Figure C-2 shows the resulting effect on the capillary pressure curve.

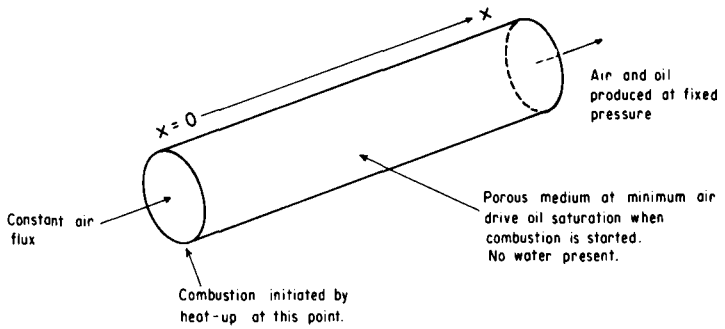

FIG. 1–LINEAR SYSTEM SIMULATED BY THE TWO-PHASE MATHEMATICAL MODEL OF FLUID FLOW DURING IN SITU COMBUSTION.

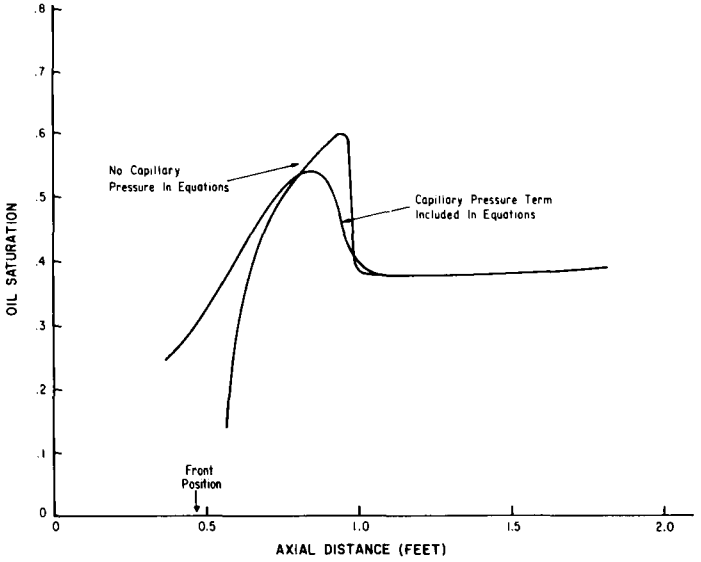

FIG. 2--'OIL BANK' DIFFICULTIES IN THE MODEL.

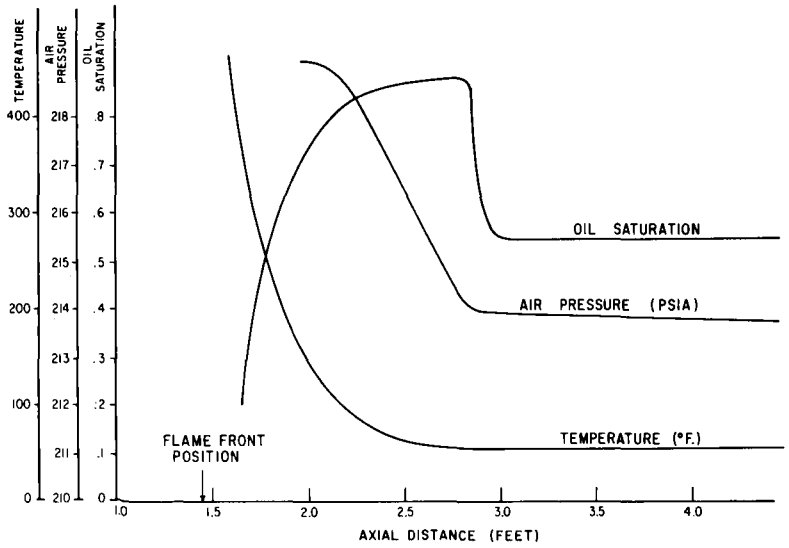

FIG. 3--TYPICAL 'OIL BANK' DEVELOPMENT IN THE MODEL .

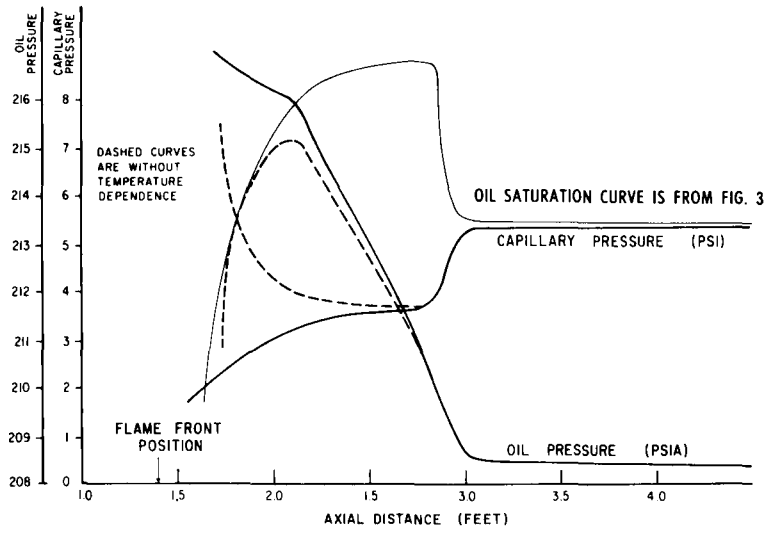

FIG. 4--EFFECT OF TEMPERATURE PRESSURE IN THE OIL PHASE.

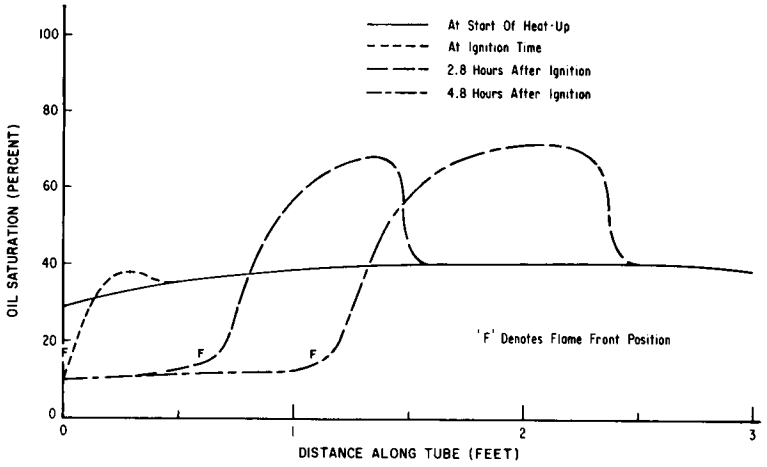

FIG. 5--OIL SATURATION DISTRIBUTION AT VARIOUS STAGES IN THE MODEL.

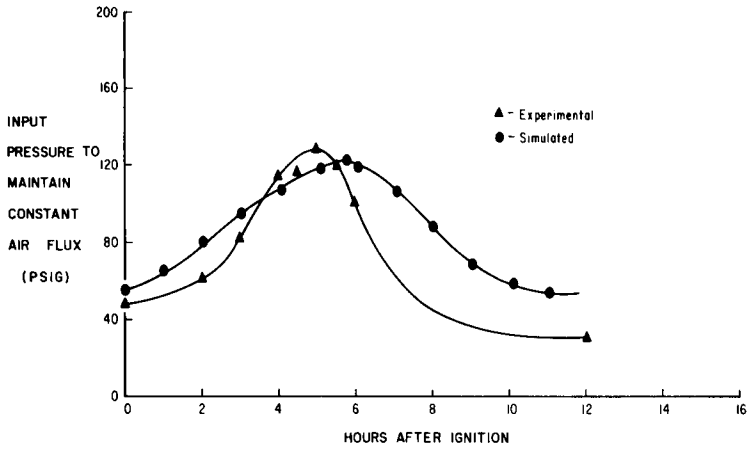

FIG. 6--RESULTS OF EXPERIMENTAL AND SIMULATED LABORATORY COMBUSTION TUBE RUNS.

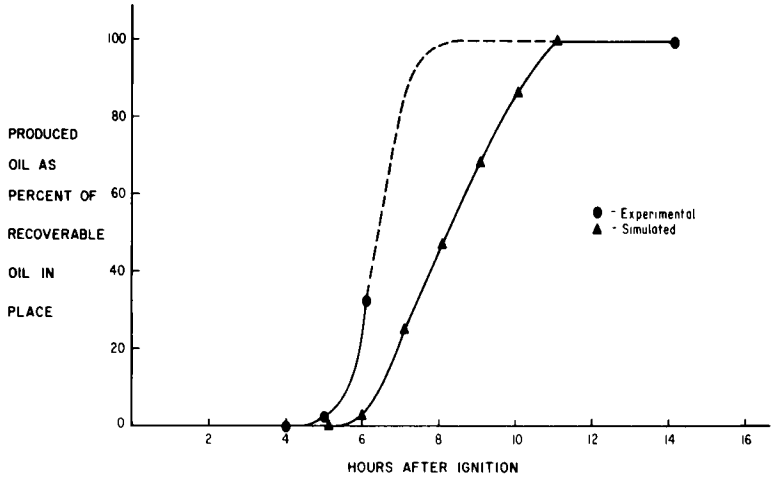

FIG. 7--RESULTS OF EXPERIMENTAL AND SIMULATED LABORATORY COMBUSTION TUBE RUNS.

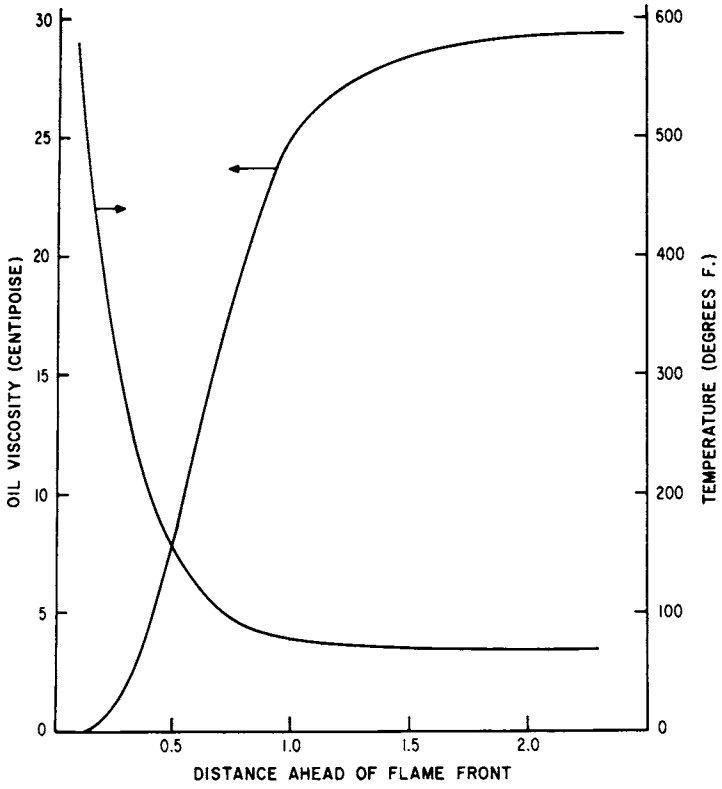

FIG. C-1--TYPICAL OIL VISCOSITY AND TEMPERATURE PROFILES.

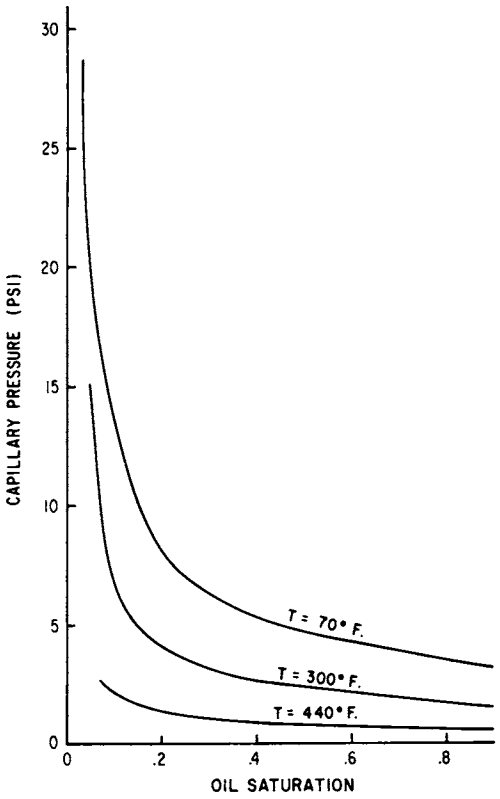

FIG. C-2--CAPILLARY PRESSURE AS A FUNCTION OF TEMPERATURE AND OIL SATURATION.